IMPACT OF LARGE DEFORMATIONS OF WEBS TRANSITING ROLLERS

By

Jinxin Shi, Ron E. Markum and J. K. Good
Oklahoma State University
USA

ABSTRACT

Webs are subjected to large out-of-plane deformations when transiting rollers in process machinery. Webs are often treated as membranes in analysis but become subject to significant bending strains when transiting rollers. Anticlastic bending of thick plates is a known phenomenon. The anticlastic effect is often ignored for webs which are thin. The objective of this paper is to demonstrate that the large bending deformations webs are subjected to on rollers influence the internal membrane stresses and deformations in the web. The results will show that the concept of normal entry of a web to a roller has complexity that has previously not been considered. It will be demonstrated that a cross direction tensile membrane stress results from the large deformations that acts to stabilize the web and inhibit wrinkle formation.

INTRODUCTION

Webs transiting rollers in roll-to-roll (R2R) process machinery is a common occurrence. Thin webs often appear to transit over rollers nicely. The web moves from a planar state in the entering span to a cylindrical shape on the roller and then resumes the planar state in the exiting span. For the most part the web is able to do this successfully. Only when the web becomes visibly unstable in the entering span (troughs) or on the surface of rollers (wrinkles) does concern arise. What is required of the web to assume the shape of a roller?

If the web is treated using simple plate theory, the internal moments required to make the web conform to the radius of a roller can be estimated [1]. Polyester film has a modulus E of 4.9 GPa (712,000 psi) and Poisson's ratio ν of 0.3. The edge moment per unit length M_x that would be required to bend a polyester film

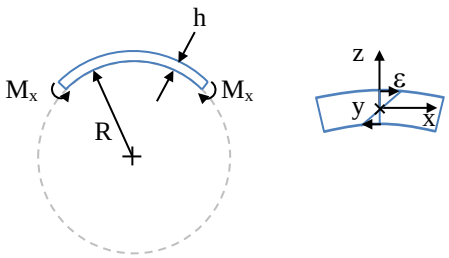

Figure 1 – Bending a Web to the Radius of a Roller

of thickness *h* 25.4 μm (0.001 in) and width *W* of 15.24 cm (6 in) to a roller radius of 3.68 cm (1.45 in) would be:

$$M_x = \frac{D}{R} = \frac{Eh^3}{12R\left(1-\nu^2\right)} = \frac{4.9*10^9*\left(25.4*10^{-6}\right)^3}{12*0.0368*\left(1-0.3^2\right)} = 1.999*10^{-4}\,N-m/m \qquad \{1\}$$

This rather small bending moment induces a bending strain that is tensile on the upper surface of the web and compressive on the lower surface. In the absence of friction, these MD strains can be calculated per Euler as:

$$\varepsilon_{MD} = \frac{z}{R} = \frac{25.4*10^{-6}/2}{0.0368} = \pm 3.45*10^{-4} \qquad \{2\}$$

The bending strain and deformation of a web is more complex than this. The Poisson effect will induce CMD strains that will be compressive on the upper surface of the web and tensile on the lower surface, and will vary linearly between the web surfaces. The CMD strains will induce curvature in the web in the CMD, a curvature which is opposite in sign to the MD curvature needed to make the web conform to the roller. This phenomenon is called anticlastic bending [2, 3]. In the example, an assumption of a wrap angle (WA) of π/2 radians will be added. The out-of-plane anticlastic deformation of a plate loaded with edge moments M_x ($1.999*10^{-4}$ *N-m/m*) is [1]:

$$w = -\frac{M_x}{2D(1-\nu^2)}x^2 + \frac{\nu M_x}{2D(1-\nu^2)}y^2 \qquad \{3\}$$

$$w(cm) = -0.1492x^2 + 0.0448y^2 \qquad \{4\}$$

where *x* and *y* are input in units of cm. The deformed web shape is shown in Figure 2. A moment was input to force the web to take the shape of a cylindrical roller. As a result of anticlastic bending, it is shown the deformed shape is not cylindrical.

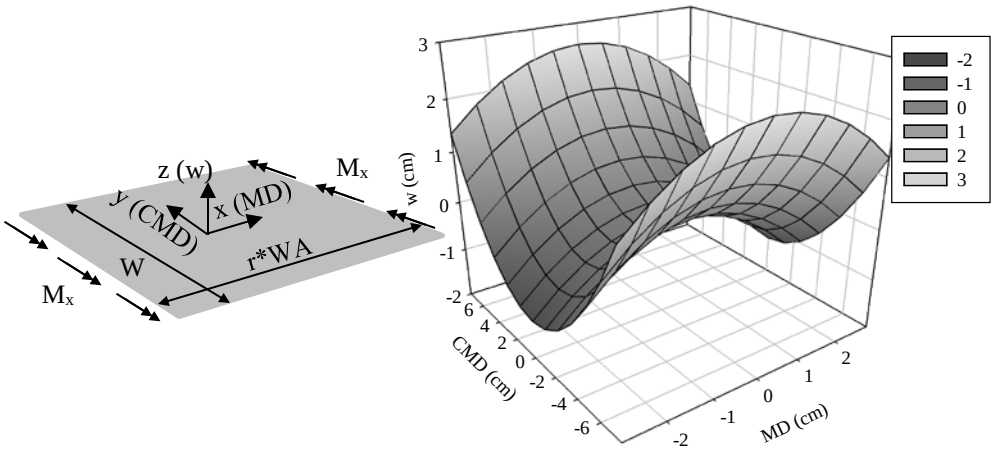

Figure 2 – Bending a Web to Conform to a Roller

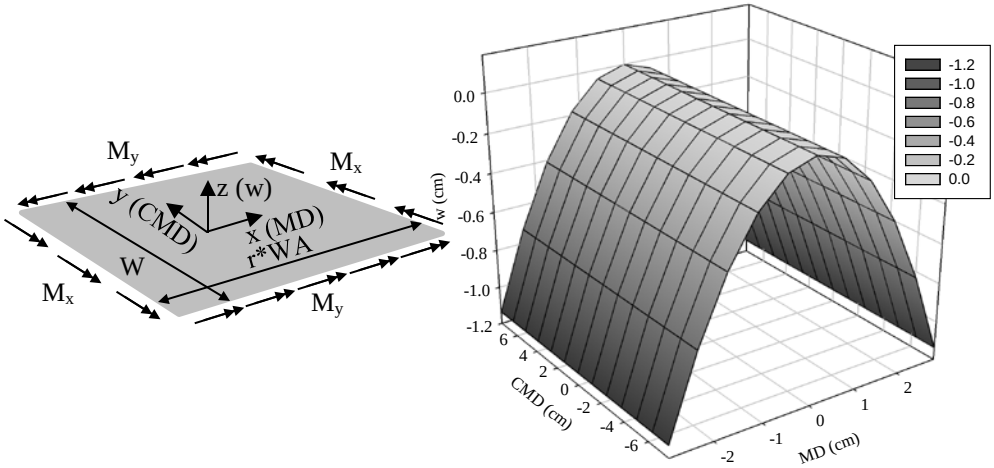

Figure 3 – Dual Moments Required to Make a Web Conform to a Roller

What applied moments would be required in the example to deform the web to a cylindrical shape that would be compatible with the shape of the roller? If edge moments are applied on all the edges of the plate, the equation for the out-of-plane deformation is:

$$w = -\frac{M_x - \nu M_y}{2D(1-\nu^2)}x^2 - \frac{M_y - \nu M_x}{2D(1-\nu^2)}y^2 \qquad \{5\}$$

If the edge moment M_y is set to the value νM_x ($5.997*10^{-5}$ *N-m/m*) Equation {5} becomes:

$$w = -\frac{M_x}{2D}x^2 = -0.1358x^2 \qquad \{6\}$$

The deformation of the web has now become a cylindrical surface as shown in Figure 3. The radius of this cylindrical surface would be:

$$\frac{1}{r_x} = -\frac{\partial^2 w}{\partial x^2} = \frac{M_x}{D} = 27.15\ m^{-1} \quad r_x = 3.68\ cm \qquad \{7\}$$

Thus, the deformed web has achieved the radius of the roller in the example (3.68 cm). Bending stresses have been induced in the web by the edge bending moments M_x and M_y which vary linearly through the web thickness. On the inner and outer surfaces these bending stresses are:

$$\sigma_{x,\mathrm{MD}} = \pm\frac{6M_x}{h^2} = \pm\frac{6\times 1.999\times 10^{-4}}{\left(2.54*10^{-5}\right)^2} = \pm 1859\ KPa$$
$$\sigma_{y,\mathrm{CMD}} = \pm\frac{6M_y}{h^2} = \pm\frac{6\times 5.997\times 10^{-5}}{\left(2.54*10^{-5}\right)^2} = \pm 558\ KPa \qquad \{8\}$$

These stresses are tensile on the outer surface of the web and compressive on the inner surface that would be in contact with the roller surface. Note, as a result of the constant bending moments M_x and M_y, these stresses are constant over the inner and outer surface of the web. The equations for stress {8} neglect any frictional forces that might be present between the web and roller.

This simple example has demonstrated the duress to which a web is subjected to conform to the surface of a roller. A web under tension transiting a roller is a more complex case and will be subject to contact pressure and frictional forces. Webs do not have applied M_x and M_y moments; they only have web tension, contact pressure between the web and roller due to tension and frictional forces applied. How does the anticlastic behavior shown for discrete sheets apply to nearly continuous webs transiting rollers in process machines? A thorough examination of the dynamic interaction of a web with a roller was in order.

FINITE ELEMENT (FE) MODEL SETUP

To explore the interaction between a web and aligned rollers, a dynamic finite element simulation of a web transiting four rollers was developed as shown in Figure 4. The simulations were run using Abaqus Standard in an implicit quasi-static mode. The web is shown at the beginning of the simulation in Figure 4. The web material properties, width and thickness are that of the example in the Introduction. The web was modeled with square SR4 shell elements with an edge dimension of 0.635 cm (0.25 in) which yielded converged results. The web span lengths between rollers (S) were all set at 45.72 cm (18 in). This provided a span ratio (L/W) of 3. The rollers were modeled as rigid analytical surfaces that were free to rotate on their axes of rotation. The radius of these rollers was selected as 3.68 cm (1.45 in) identical to the roller used earlier in the example. At the start of the simulation, the shell elements defining the web on the rollers are cylindrical shells with an inside radius equal to the outside radius (3.68 cm) of the roller. An entry span length of web 215.9 cm (85 in) long was modeled prior to roller R1. When the simulation begins, the shells of web on the rollers transit out into the free spans. Bending stresses are induced that can induce transient motion when these sections of web

pass each roller. The benefit of the long entry span length is that by the conclusion of the simulation all of these sections of the web that began on the rollers have passed downstream of roller R4 and will not affect the final results. The coefficient of the friction (COF) between the web and the rollers was set at 0.4. During the first 0.1 s of the simulation, the downstream velocity is maintained at zero while the web tension was increased to 3.45 MPa (500 psi) and then held constant through the remaining 29 s of the simulation. After the stress due to web tension stabilized, the downstream web velocity was increased from zero to 7.37 cm/s (2.9 in/s) in 0.5 s and maintained constant through the duration of the simulation.

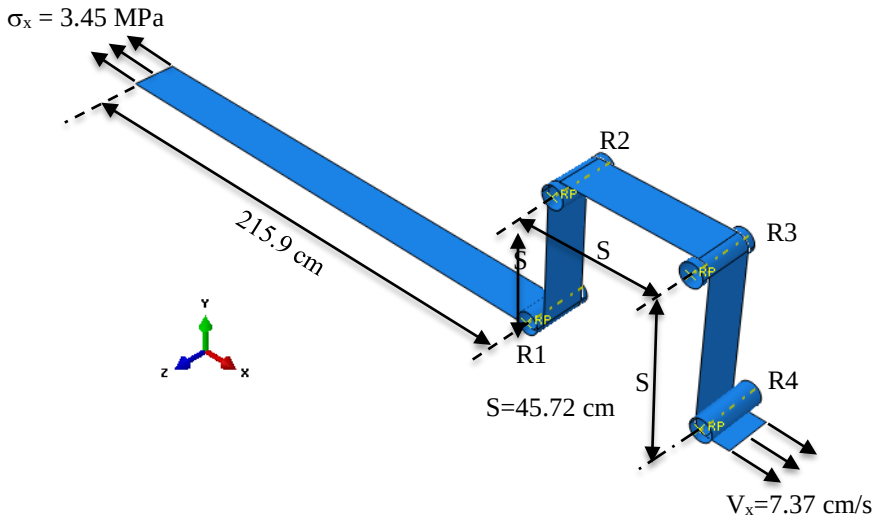

Figure 4 – Finite Element Model Setup

SIMULATION RESULTS AND DISCUSSIONS

The web stresses achieve a steady state level very quickly in these simulations. The maximum CMD membrane stress on roller R3 is shown in Figure 5. Results are being shown for a case where Poisson's ratio was set to 0.3. The stress is close to zero as the web begins to move, it then increases rapidly for about 2 seconds as shown in Figure 5. After 2 seconds, this stress becomes nearly constant with only small variations. The maximum CMD membrane stresses on all rollers are very similar in magnitude and in the way in which they vary through time. The time required for a point on the web to move from entry to exit of a roller is 0.784 s. This is the dynamic time constant for these simulations. After 3 time constants (2.35 s), near steady state behavior should be expected in these simulations and is shown to be the case in Figure 5.

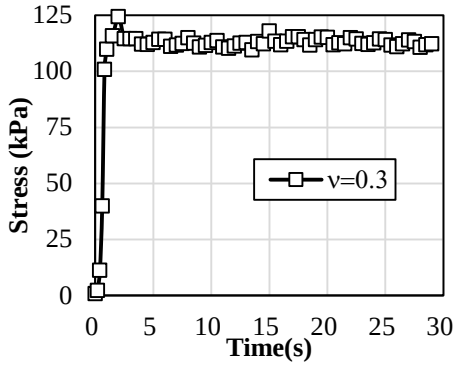

Figure 5 – Maximum CMD Membrane Stress on R3

The existence of the CMD tensile membrane stress shown in Figure 5 is interesting and indicates that the interaction of the web with the cylindrical roller has a stabilizing or spreading influence on the web. This is the first quantitative proof that cylindrical rollers have a spreading effect on webs. Previously empirical proof was given that a misaligned cylindrical roller was superior in resisting web wrinkles than cylindrical rollers with tape wound in a spiral inward or outward pattern [3]. The origin of this tensile CMD stress will be explored further.

The plate theory example demonstrated that a moment M_y of magnitude νM_x should be applied to the web edges to cause the CMD curvature due to the anticlastic effect to vanish and allow the web to assume a cylindrical shape while transiting the roller. From Equation {8}, the CMD bending stresses were shown to have a linear variation through the web thickness. These stresses should be positive on the outer surface, zero on the neutral surface, and negative on the inner surface where the web in contact with the roller. These stresses should be constant across the web width provided the moment M_y is constant across the web width. After steady state conditions are achieved in the simulation, the CMD bending stresses approach 655 KPa (95 psi) on the outer surface, 110 KPa (16 psi) at the mid-plane, and -448 KPa (-65 psi) on the inner surface as shown in Figure 6. Note in Figure 6, the CMD stresses on the inner and outer surface are essentially constant across the web width. The 655 KPa CMD stress on the outer surface is comparable to the 558 KPa stress predicted in Equation {8}. The 113 KPa CMD tensile membrane stress at the mid-plane was unexpected and the -448 KPa stress is comparable to the -558 KPa value from Equation {8} for the inner surface value. The CMD stresses at the inner and outer surfaces and the mid-plane are all approximately 100 KPa larger than expected from plate theory. What is clear in Figure 6 is that constant CMD bending stresses are experienced across the web width in the simulation that are similar to those witnessed in the plate theory example. This demonstrates that even though webs are thin that they are subjected to considerable bending strain during transit over rollers and that the effects of anticlastic bending are present and significant. The CMD stresses shown in Figure 6 are very similar on all four rollers (R1 through R4).

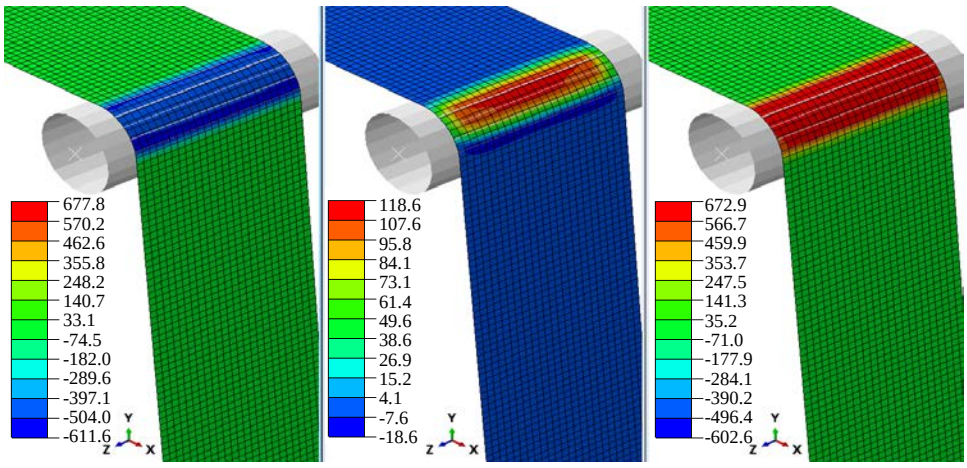

inner surface mid-plane outer surface

Figure 6 – CMD Stresses (KPa) on R3 ν = 0.3

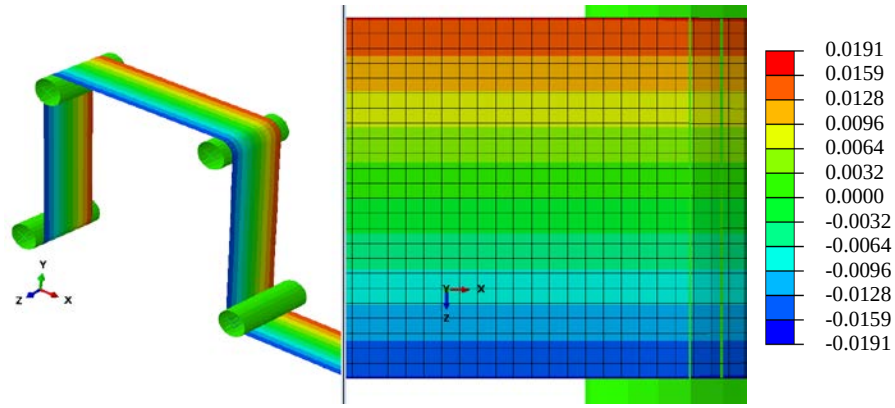

Whole model Web entering R3

Figure 7 – CMD Displacements on R3 (mm) ν = 0.3

To explore the origin of the CMD spreading stresses witnessed at the mid-plane of the web on the rollers, the CMD deformations were examined. When a flat web is subjected to MD tension with no CMD constraint, the web would have a uniform CMD contraction due to the Poisson effect. For the web simulated the uniform contraction expected would be 3.45 MPa/4.9 GPa*0.3*15.24 cm/2 or 0.016 mm, again for the case where Poisson's ratio was 0.3. In the simulations conducted, the web takes the shape of a cylindrical surface while transiting over a roller but the anticlastic effects, any attempt to gain normal entry and friction forces would cause the lateral contraction to deviate from the uniform level. As shown on the left in Figure 7, the CMD displacements appear to be uniform and exhibit symmetric width reduction of the web edges at the macro level. However, the zoomed figure on the right shows deviation in the CMD displacements as

the web enters roller R3. The web edges contract slightly more while transiting the roller compared to the contraction in the free span. This additional contraction is shown clearly in the displacements of the web edge shown in Figure 8. The markers filled in black indicate the locations where the web enters or exits one of the four rollers. Although the difference of the displacements where the web on the roller and in the free span is not huge, it indicates the web has nonzero slope at edges when it enters the roller.

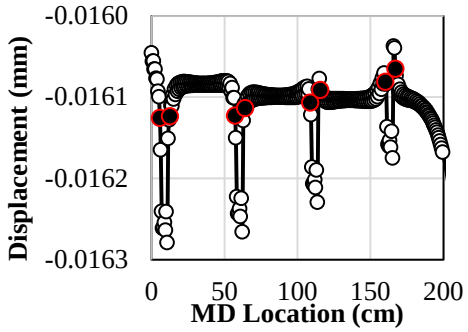

Figure 8 – The lateral Displacement of the +z Web Edge ($\nu = 0.3$)

The slope of the web at the entry to the roller is determined by a central finite difference approximation to acquire the first order differentiation of the CMD displacements with respect to the MD coordinates. The nodes of an SR4 shell element have 6 degrees of freedom which include three translations along the xyz axes in Figure 7 as well as rotations about those axes. Differentiation of the lateral displacements provides superior estimate with less numerical noise than the out-of-plane rotations which are output. The web contracts in the CMD upon entry to the roller, which was evident in Figure 8. The slope at web entry is positive on the –z web edge and negative on the +z edge. The *concept of normal entry* dictates a web should enter the roller normal to the axis of rotation, which means the slope should be zero. The concept of normal entry is based completely on kinematics without regard for the frictional forces between the web and roller needed to sustain the zero slope or for the higher order deformations that occur in the web due anticlastic bending. The concept of normal entry has been applied in numerous circumstances in web lateral mechanics and dynamics investigations. In these investigations, the web is modeled as a beam. The concept of normal entry is applied at the elastic axis of the beam at entry to a downstream roller and may be used to determine a steady state lateral behavior. The method for estimating the slope at the entry to the roller is shown in Figure 9. The slope is estimated at the CMD line of nodes closest to the web entry.

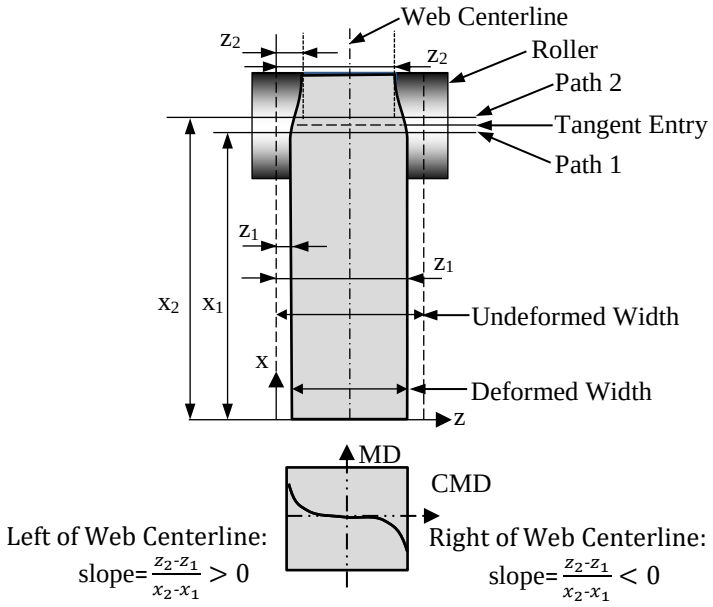

Figure 9 – The Entry Slope of the Web at the Roller

The result of the estimation is shown in Figure 10 for the case where Poisson's ratio of the web is 0.3. Note at the widthwise center of the web that the entry slope is very close to zero (the estimate was $5.5*10^{-14}$ rad). The slopes at the web edges were significantly larger ($\pm$ $6.25*10^{-6}$ rad). Also note that the integrated average of the slope over the web width would be essentially zero. Thus for analyses where the web is modeled as a beam, the normal entry boundary condition appears appropriate if sustainable by available friction. Note the signs of the slope at the web edges will promote spreading and are responsible for the CMD tensile spreading stresses witnessed on the mid-plane in Figures 5 and 6.

The slope is shown spatially in Figure 11 prior to entry, on the roller and exiting roller R3. The potential for some slip always exists as a web enters and exits a roller due to the normal contact pressure being very small at the tangent entry and exit and the finite bending stiffness of the web. In Figure 11 slip is occurring at the entry and exit as the MD strain on the inner transitions from the membrane value in the free span, to a lower value due to the bending strain shown in Equation {2} but reduced by friction and returning to the membrane value at the exit. In these same regions lateral slip and occur as well. The slope of the web is much diminished in Figure 11 between the entry and exit regions where stick behavior was predominant. The slip in the entry and exit regions as well as the stick behavior between those regions was evident in the contact status output from Abaqus.

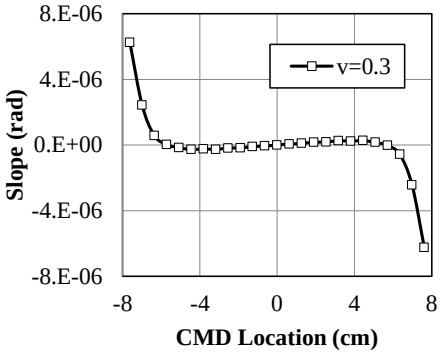

Figure 10 – Entry Slope at R3

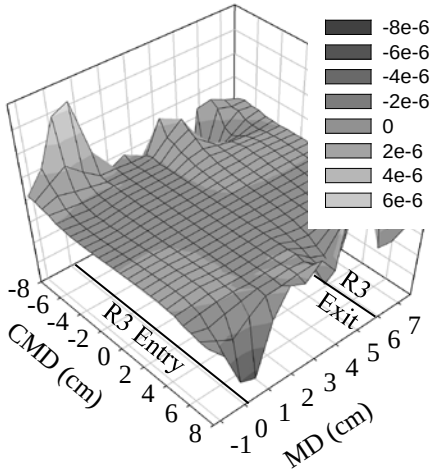

Figure 11 – Slope (rad) on Roller R3

The CMD spreading stresses witnessed in Figures 5 and 6 and the non-zero web entry slopes that caused those stresses were hypothesized to be the result of the anticlastic deformations described in the example in the introduction. Partial proof of the hypothesis was provided by the constant CMD stresses that were nearly constant across the web width in the simulations (Figure 6) and comparable to those predicted from Equation {8} on the inner and outer surfaces. Further proof was sought by conducting additional simulations while varying only Poisson's ratio. As Poisson's ratio approaches zero, the anticlastic deformation should vanish per Equation {3}. The results of those simulations are shown in Figure 12. The CMD spreading stress did vanish when Poisson's ratio was zero. Furthermore, there appeared to be near proportionality of the CMD spreading stress as a function of Poisson's ratio. The average of the steady state CMD spreading stresses at the mid-plane surface are shown as a function of Poisson's ratio in Figure 13. A linear fit of the averaged data was performed and the correlation coefficient is close to unity. Thus from the simulations it has been proven that the CMD mid-plane spreading stresses are (1) the result of anticlastic bending and (2) are proportional to Poisson's ratio.

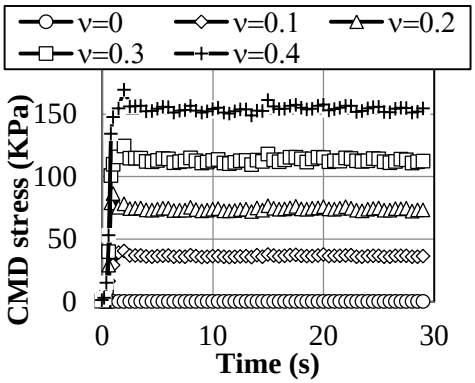

Figure 12 – Effect of Poisson's Ratio on CMD Mid-Plane Stress.

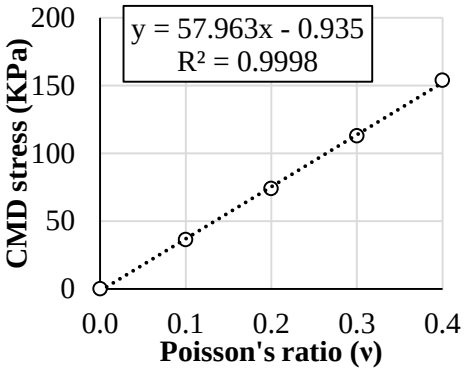

Figure 13 – Dependence of CMD Spreading Stress on Poisson's Ratio.

The CMD stresses on the inner, mid-plane and outer surfaces are shown in Figure 14 for the case where Poisson's ratio was set to zero. The anticlastic effect is no longer present. The CMD stresses at the mid-plane and the inner and outer surfaces have vanished.

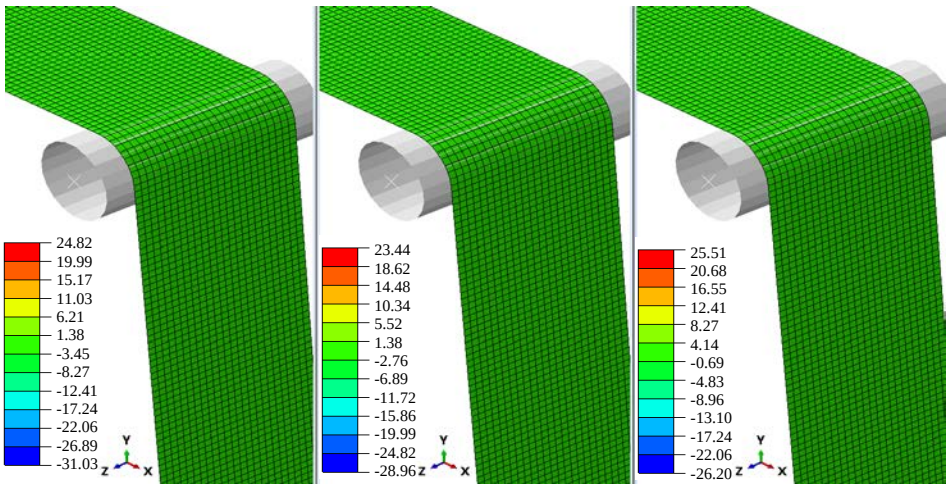

Inner surface Mid-plane surface Outer Surface

Figure 14 – Vanishing of CMD Stresses (Pa) on R3 for Zero Poisson's Ratio

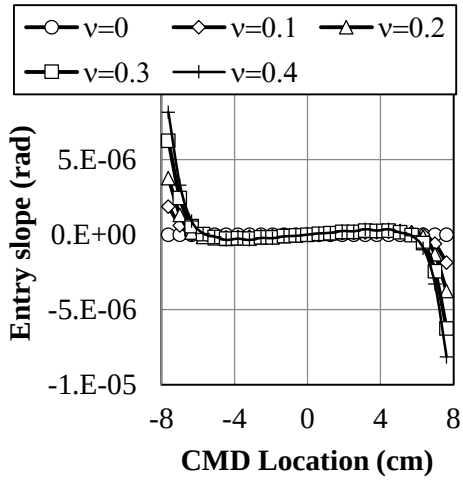

Figure 15 – Effect of Poisson's ratio on entry slope.

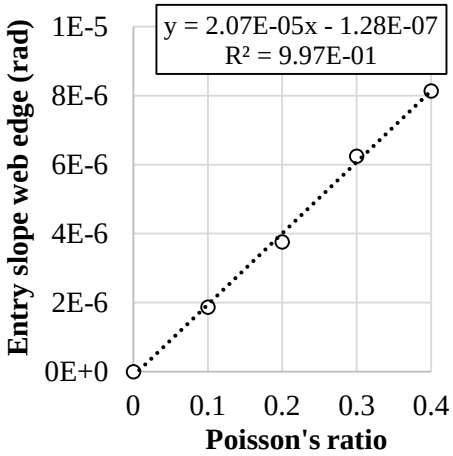

Figure 16 – Effect of Poisson's ratio on web edge entry slope.

The entry slope of the web as for various levels of Poisson's ratio is shown in Figure 15. Note when Poisson's ratio is zero that the entry slope is zero at all CMD locations and is indicative of why the spreading stresses for this case in Figures 12 and 14 were also zero. Note with increasing Poisson's ratio the entry slopes at the web edges are also increasing. The absolute value of the edge entry slopes are shown in Figure 16 as a function of Poisson's ratio. A linear curve fit of the slope data is shown that yielded a high correlation coefficient (0.997). Thus, the entry slope at the web edge (Figure 16) and the mid-plane CMD spreading stresses (Figure 13) have been shown to be proportional to Poisson's ratio.

EXPERIMENTAL VERIFICATION

The results from anticlastic theory (Equation {8}) and simulation results (Figure 6) indicate that a web with Poisson's ratio greater than zero would have a tensile CMD stress on outer surface of the web as the webs transits a roller. Good agreement was seen for the MD and CMD bending stresses on the inner and outer surfaces produced by the simulations of the 25.4 μm web and the closed form equations for the four-roller web case. Further verification was sought to determine if the stresses due to anticlastic behavior could be measured in the laboratory.

A polyester web 0.254 mm (0.01 in.) in thickness and 15.24 cm (6 in.) wide was chosen to explore the anticlastic effect in the laboratory. The modulus of elasticity of the web was measured and found to be 4.89 GPa (710,000 psi) and Poisson's ratio was found to be 0.36. The strains were measured using strain gages adhered to the web surface. The strain gages[1] had a polyimide backing that was 7.9 mm (0.31 in.) square and 76.2 μm (0.003 in) in thickness. The web was 3.3 times thicker than the strain gages and was chosen to reduce the effects of reinforcement of the web by the strain gage. The web instrumented with strain gages was positioned to transit a roller 5.08 cm (2 in.) in radius on the High Speed Web Line in the Web Handling Research Center. The coefficient of friction between the roller and the web was measured to be 0.24. As shown in Figure 17,

[1] CEA-06-062UT-350, Micro-Measurements, POB 27777, Raleigh, NC, 27611, USA.

the strain gauge was bonded to the web at the CMD center. The strain gages had two elements (90¬ tee rosette pattern) and will allow the measurement of the MD and CMD strains of the web simultaneously. Gage tabs were used as shown in Figure 17 such that the bending stiffness of the lead wires was minimized in the vicinity of the strain gage. The leads were connected to a multichannel strain conditioner/amplifier[2] whose output was input to a data acquisition system[3]. A fiber optic sensor[4] was used to sense when the center of the strain gage resistance grids passed the tangent entry of the web to the roller.

A finite element (FE) simulation similar to that described earlier but with the web and roller properties used in the test was developed as shown in Figure 18. In the test, the strain gauge grid was centered and bonded on the web centerline. A cyanoacrylate adhesive[5] was used and the total thickness for the web, adhesive layer and the strain gauge is 0.335 mm (0.0132 in.). In the simulation, the web was modelled with a local increase in thickness in the location of the strain gage to account for the local increase in stiffness due to the installation of the gage. The lead wires were not considered, their bending stiffness was assumed to be negligible. During tests, the web tension was maintained at 214 N (48 lb). This induced an MD membrane stress of 5.52 MPa (800 psi) which was applied as a surface traction on the upstream end of the web. The downstream end of the web was brought to an MD velocity of 3.05 mpm (2 ips) consistent with the experiment.

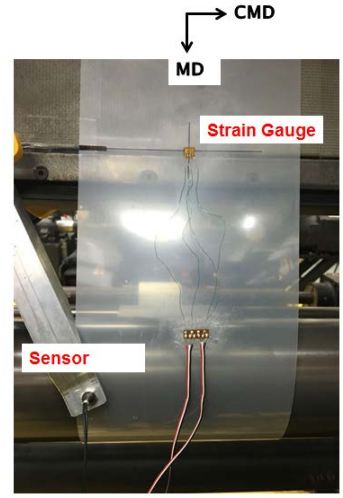

Figure 17 – Experiment setup

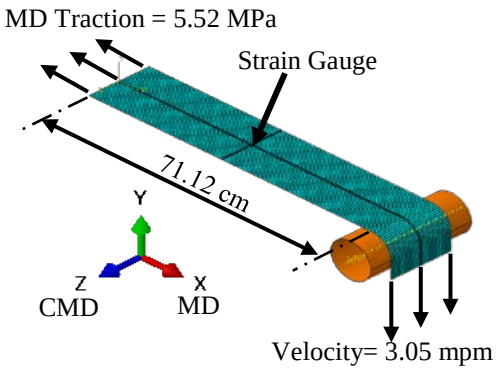

Figure 18 – Simulation of tests

In this simulation, the MD stress on the web outer surface rises quickly from 5.52 MPa (800 psi) in the free span to 19.65 MPa (2850 psi) on the roller as shown in Figure

[2] 2100 System, Micro-Measurements, POB 27777, Raleigh, NC, 27611, USA.
[3] PCIe 6251, National Instruments, 11500 N Mopac Expressway, Austin, TX 78759-3504, USA.
[4] FS-V11, Keyence Corporation, 500 Park Boulevard, Suite 200, Itasca, IL 60143, USA.
[5] MBOND-200, Micro-Measurements, POB 27777, Raleigh, NC, 27611, USA.

19. Theoretically the moment required to bend the test web to the radius of the test roller is:

$$M_x = \frac{D}{R} = \frac{Eh^3}{12R\left(1-\nu^2\right)} = \frac{4.89*10^9*\left(254*10^{-6}\right)^3}{12*0.0508*\left(1-0.36^2\right)} = 0.151N-m/m \qquad \{9\}$$

The bending stress in the outer surface would be:

$$\sigma_{MD} = \sigma_{MD,\,free\ span} + \frac{6M_x}{h^2} = 5.52 + \frac{6*0.151}{\left(254*10^{-6}\right)^2 10^6} = 19.6\ \text{MPa} \qquad \{10\}$$

This is within 0.3% of the simulation result.

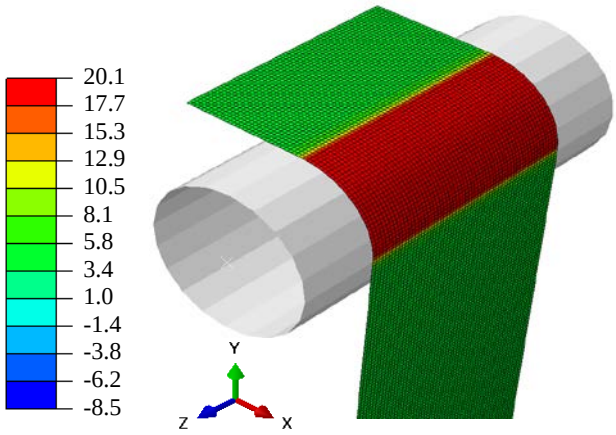

Figure 19 – The MD Stress (MPa) on the Outer Surface

The CMD stresses that result from bending the anticlastic surface so that it is compatible with the cylindrical surface of the test roller can be determined using Equation {8}:

$$\sigma_{y,CMD} = \pm\frac{6M_y}{h^2} = \pm\frac{6\nu M_x}{h^2} = \pm\frac{6*0.36*0.151}{\left(254*10^{-6}\right)^2 10^6} = \pm 5.05\ \text{MPa} \qquad \{11\}$$

Thus if the reinforcement of the strain gauge is not considered, the CMD stress the outer surface of the web on the roller is 5.05 MPa (733 psi), zero at neutral surface and -5.05 MPa on the inner surface according to the Equation {11}. The stress variation through the web depth is quite similar to the simulation results shown in Figure 20. The simulation stresses were harvested on a path half way through the wrap angle of the web on the roller. A tensile CMD spreading stress of 50 KPa was witnessed at the mid-plane in the simulation.

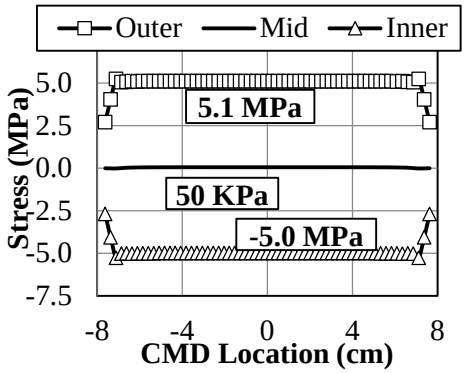

Figure 20 – CMD Stresses from Simulation

The MD and CMD strains of the web in the free span $\varepsilon_{MD,free}$, $\varepsilon_{CMD,free}$ and on the roller ε_{MD}, ε_{CMD} can be estimated using the constitutive Equation {12}. As the web moves from the free span onto the roller, the MD strain on the outer surface (ε_{MD}) would increase from 1129 to 3636 μm/m. The CMD strain on the outer surface changes very little, from -406 μm/m in the free span to -410 μm/m on the roller surface.

$$\begin{aligned}
\varepsilon_{MD,\,free} &= \frac{\sigma_{MD,\,free} - \nu\sigma_{CMD,\,free}}{E} = \frac{5.52 - 0.36*0}{4890} = 1129\mu m/m \\
\varepsilon_{CMD,\,free} &= \frac{\sigma_{CMD,\,free} - \nu\sigma_{MD,\,free}}{E} = \frac{0 - 0.36*5.52}{4890} = -406\mu m/m \\
\varepsilon_{MD} &= \frac{\sigma_{MD} - \nu\sigma_{CMD}}{E} = \frac{19.6 - 0.36*5.05}{4890} = 3636\mu m/m \\
\varepsilon_{CMD} &= \frac{\sigma_{CMD} - \nu\sigma_{MD}}{E} = \frac{5.05 - 0.36*19.6}{4890} = -410\mu m/m
\end{aligned} \qquad \{12\}$$

The strains from Equation {12} do not account for the reinforcement of the strain gage, the friction and potential for slippage between the web and roller and the steering/spreading effects of forcing the anticlastic surface of the web to acquire the cylindrical shape of the roller. These factors were all accounted for in the simulation. In the simulation, the MD and CMD strains were recorded at the center of the strain gauge through time. As shown in Figure 21, the MD strains from the simulation and experiment match quite well. The CMD strain remain nearly constant, which is consistent with Equation {12}, while the MD strains increase significantly as the strain gauge moves from the free span onto the roller. The bending strains in the outer surface of the web from tests and simulations are about 4000 μm/m, in excess of the 3636 μm/m from {12}. This was expected due the added thickness of the strain gage atop the web.

The experimental MD and CMD stresses on the web outer surface can be inferred using the plane stress Equation {13} and the experimental strains:

$$\begin{aligned}
\sigma_{MD} &= \tfrac{E}{(1-\nu^2)}[\varepsilon_{MD} + \nu\varepsilon_{CMD}] \\
\sigma_{CMD} &= \tfrac{E}{(1-\nu^2)}[\varepsilon_{CMD} + \nu\varepsilon_{MD}]
\end{aligned} \qquad \{13\}$$

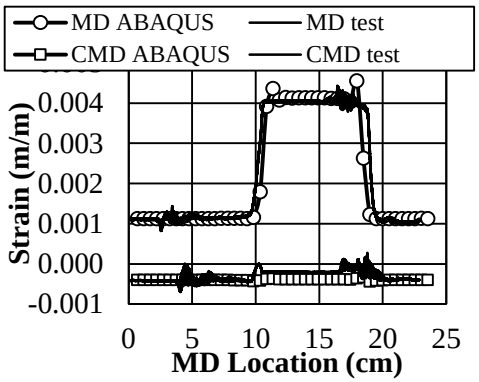

Figure 21 – Strain: Simulation and Test

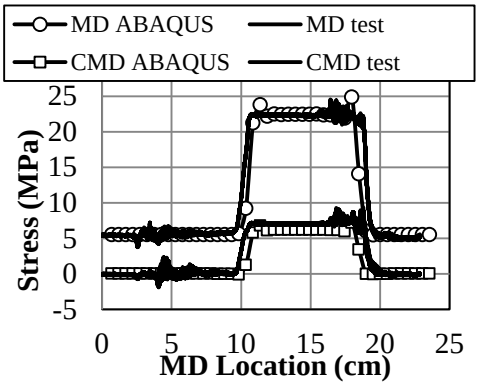

Figure 22 – Stress: Simulation and Test

The MD and CMD test and simulation stresses on the web outer surface agree well and are shown in Figure 22. Tensile CMD stresses of consequence are witnessed in the web on the roller, which is experimental proof that anticlastic effects exist in thin webs. From Equation {10}, the MD stress on the web outer surface is 19.6 MPa on the roller without considering strain gauge, and it is 5.52 MPa in the free span as set in the simulation. In Figure 22, the MD stress on the roller from tests and simulation are 22 MPa, larger than that from Equation {10} due to the added thickness of the gage and the inability of Equation {10} to encompass the effects of friction and slippage. The CMD stresses on the web outer surface on the roller are 5.05 MPa from Equation {11} and 5.1 MPa from the Figure 20 for the case with no strain gage. The results in Figure 22 are slightly larger but again this was expected because of the added thickness of the strain gage.

CONCLUSIONS

Anticlastic bending produces measurable and beneficial effects for webs transiting rollers. Anticlastic effects are commonly considered negligible for thin palates such as webs. This consideration is based on the notion of small deflections where the out-of-plane deflections are comparable to the thickness of the plate. Webs transiting rollers undergo bending deformations that can be thousands of times greater than their thickness. In free space a web bent to the radius of a roller on one axis does desire to take an anticlastic shape as shown in Figure 2. Web tension is often sufficient to cause the web to conform and become compatible with the surface of rollers. The web tension and the resulting web deformations do result in inducing M_y internal moments (Figure 3) as proven by the constant CMD stresses on the inner and outer surfaces across the web width (Figures 6 and 20). Anticlastic bending does result in non-normal entry of the web away from the CMD center of the web (Figure 15). This resulted in tensile CMD spreading stresses on the mid-plane of the web (Figures 12 and 20). It was shown that the slope of the web edge at the tangent entry (Figure 16) and the CMD spreading stresses acting at the mid-plane (Figure 13) were proportional to Poisson's ratio. When Poisson's ratio became zero, normal entry was achieved at all CMD locations across the web width (Figures 15 and 16) and the CMD spreading stress vanished (Figures 12 and 13) which provided evidence the behaviors were the result of anticlastic bending.

The example web studied showed the web width contracted on the order of 100 μm in Figure 8 from web center to edge. This may present challenges for industries concerned with the precision printing and registration of electronics.

The dynamic finite element simulations have provided perhaps the best understanding to date of the *concept of normal entry* of a moving web approaching contact to a downstream roller. The theory of Timoshenko [2], dynamic finite element simulation and experimental validation have proven the effects of anticlastic bending exist in common webs in roll-to-roll process machines. While the CMD mid-plane spreading stresses are beneficial in resisting web wrinkling, no simple closed form equations will allow their calculation since they are the result of slippage and non-normal entry of the web.

ACKNOWLEDGMENTS

Portions of this work were supported by the National Science Foundation under Grant 1635636 and by the Web Handling Research Center of Oklahoma State University. Any opinions, findings, and conclusions or recommendations expressed in this material are those of the author(s) and do not necessarily reflect the view of the National Science Foundation.

REFERENCES

1. Timoshenko, S. P., Woinowsky-Krieger, S., Theory of Plates and Shells, 2nd Ed, McGraw-Hill, New York, 1959, p. 5.
2. Timoshenko, S. P., Woinowsky-Krieger, S., Theory of Plates and Shells, 2nd Ed, McGraw-Hill, New York, 1959, pp. 33-45.
3. Ashwell, D. G., "The Anticlastic Curvature of Rectangular Beams and Plates," Journal of the Royal Aeronautical Society, Vol. 54, No. 479, 1950, pp. 708- 715.
4. Swanson, R. P., "Testing and Analysis of Web Spreading and Anti-Wrinkle Devices," Proceedings of the Fourth International Conference on Web Handling, Web Handling Research Center, Oklahoma State University, Stillwater, Oklahoma, 1997, pp. 414-429.